Uniqueness of an inverse electromagnetic coefficient problem with partial boundary data and its numerical resolution through an iterated sensitivity equation

Jérémy Heleine

Uniqueness of an inverse electromagnetic coefficient problem with partial boundary data and its numerical resolution through an iterated sensitivity equation

Jérémy Heleine[a]

Drafted October 17, 2023

Abstract

In this paper we study an inverse boundary value problem for Maxwell's equations. The goal is to reconstruct perturbations in the refractive index of the medium inside an object from the knowledge of the tangential trace of an electric field on a part of the boundary of the domain. We first provide a uniqueness result for this inverse problem. Then, we propose a complete procedure to reconstruct numerically the perturbations, based on the minimization of a cost functional involving an iterated sensitivity equation.

Keywords: Maxwell's equations, inverse problem, uniqueness, quasi-reversibility, sensitivity equation, numerical simulations

1 Introduction

The study of microwave imaging is of great interest, with potential medical or industrial applications. The idea is to take benefits of the fact that the interaction between electromagnetic fields and a material can be described from the dielectric properties of the latter. For example, this modality is in study for medical applications like the diagnostic of strokes [18, 19]. Indeed, a stroke affects tissues of the brain, resulting in variations of their dielectric properties. The aim is then to recover these variations in order to characterize the stroke and apply the right treatment to the patient. In the same way, microwave imaging is a promising alternative to mammography [14].

Mathematically speaking, microwave imaging defines an inverse problem. Let Ω be a bounded and simply connected domain of $\mathbb{R}^p$, $p \in \{2, 3\}$, with boundary $\Gamma \coloneqq \partial\Omega$ and unit outward normal denoted by $\boldsymbol{n}$. The magnetic permeability of the medium in Ω is assumed to be the same as in the vacuum, μ_0. The electric permittivity and conductivity in the medium are two functions of the space variable $\boldsymbol{x}$, respectively denoted by ε and σ. We then define the complex refractive index by

$$\kappa \colon \Omega \ni \boldsymbol{x} \mapsto \frac{1}{\varepsilon_0}\left(\varepsilon(\boldsymbol{x}) + i\frac{\sigma(\boldsymbol{x})}{\omega}\right) \in \mathbb{C},$$

where ε_0 is the electric permittivity in vacuum and $\omega > 0$ is the (fixed) wave frequency. The electric field $\boldsymbol{E}$ in Ω then satisfies the time-harmonic Maxwell's equation

$$\mathbf{curl}\,\mathbf{curl}\,\boldsymbol{E} - k^2\kappa\boldsymbol{E} = 0, \tag{1}$$

with $k \coloneqq \omega\sqrt{\mu_0\varepsilon_0}$ being the wave number.

We are interested in the inverse boundary value problem consisting in recovering the refractive index in the whole domain Ω from the knowledge of partial surface measurements at fixed frequency. The part of the boundary $\Gamma_0 \subset \Gamma$ where measurements will be assumed to be known is called the accessible part. We assume that $\mathrm{meas}(\Gamma_0) > 0$ and we denote by $\Gamma_1 \coloneqq \Gamma \setminus \overline{\Gamma_0}$ the nonaccessible

[a]Contact: jeremy.heleine@math.univ-toulouse.fr. Institut de Mathématiques de Toulouse CNRS UMR 5219 - Université Paul Sabatier F-31062 Toulouse Cedex 9, France

part. In this paper, we study the question of the uniqueness for such a problem. We then propose an algorithm to numerically solve this inverse problem.

We assume here that the unknown function κ is a perturbation of a background refractive index, denoted by κ_0 and assumed to be known in Ω. Moreover, we assume that the perturbations are not glued to the boundary. In other words, there exists a tubular neighborhood $\mathcal{V}$ of Γ in Ω, that is:

$$\exists r_{\mathcal{V}} > 0 / \forall \boldsymbol{x} \in \Gamma, B(\boldsymbol{x}, r_{\mathcal{V}}) \cap \Omega \subset \mathcal{V},$$

where $B(\boldsymbol{x}, r_{\mathcal{V}})$ is the open ball centered at $\boldsymbol{x}$ of radius $r_{\mathcal{V}}$, such that $\mathrm{supp}(\kappa - \kappa_0)$ is contained in $\Omega \setminus \bar{\mathcal{V}}$. This assumption allows us to write $\kappa|_{\mathcal{V}} = \kappa_0|_{\mathcal{V}}$: the refractive index is known in $\mathcal{V}$. An example of such configuration is provided in Figure 1.

Assuming that the refractive index is known in a tubular neighborhood $\mathcal{V}$ of Γ has two benefits. From a theoretical point of view, it allows us to state a uniqueness result without having to fix some specific geometric nor physical conditions on the nonaccessible part of the boundary. This will be done in Section 2. From a practical point of view, this assumption also allows us to have a well-defined system for the data completion problem. In Section 3, we then propose a way to retrieve total data from partial ones: starting with data known on the accessible part of the boundary, we obtain data defined on a complete boundary. Section 4 is devoted to an application mapping amplitudes of perturbations to corresponding electric fields. We show that this application can be derived indefinitely, the value of its derivatives being given by the so called iterated sensitivity equation. An asymptotic expansion of this application is then used in Section 5 to define a regularization of a classical cost function. In Section 6, we describe a complete procedure to reconstruct perturbations from the knowledge of the electric field on the accesssible part. This procedure is then tested against different 2D and 3D configurations.

2 Uniqueness result

Let us introduce the vector space

$$H(\mathbf{curl}) \coloneqq \{\boldsymbol{u} \in L^2(\Omega)^3 \ ; \ \mathbf{curl}\, \boldsymbol{u} \in L^2(\Omega)^3\}.$$

For any vector field $\boldsymbol{u} \in H(\mathbf{curl})$, the tangential trace is defined by continuous extension of the mapping $\gamma_t(\boldsymbol{u}) = \boldsymbol{u}|_{\Gamma} \times \boldsymbol{n}$ (see for example [15]). We introduce the trace space

$$Y(\Gamma) \coloneqq \{\boldsymbol{f} \in H^{-1/2}(\Gamma)^3 \ ; \ \exists \boldsymbol{u} \in H(\mathbf{curl}) / \gamma_t(\boldsymbol{u}) = \boldsymbol{f}\},$$

and its restriction in the distributional sense to Γ_0

$$Y(\Gamma_0) \coloneqq \{\boldsymbol{f}|_{\Gamma_0} \ ; \ \boldsymbol{f} \in Y(\Gamma)\}.$$

The inverse boundary value problem we are interested in is to determine the electric permittivity ε and conductivity σ from boundary measurements taken on the accessible part Γ_0, obtained from a given boundary source term, at a fixed frequency ω. These measurements are modeled by a Cauchy data set $C(\varepsilon, \sigma; \Gamma_0)$, as defined in the following.

Definition 2.1. *The pair of coefficients ε and σ is said admissible if both are in $\mathcal{C}^1(\bar{\Omega})$, with $\varepsilon \geq \tilde{\varepsilon}$ and $\sigma \geq 0$ almost everywhere in Ω, for a constant $\tilde{\varepsilon} > 0$.*

Definition 2.2. *For a pair of admissible coefficients (ε, σ) defined in Ω as in Definition 2.1, the corresponding Cauchy data set $C(\varepsilon, \sigma; \Gamma_0)$ at a fixed frequency $\omega > 0$ consists of pairs $(\boldsymbol{f}, \boldsymbol{g}) \in Y(\Gamma_0) \times Y(\Gamma_0)'$ such that there exists a field $\boldsymbol{E} \in H(\mathbf{curl})$ satisfying (1) for $\kappa \coloneqq (\varepsilon + i\sigma/\omega)/\varepsilon_0$ with boundary conditions $\boldsymbol{E}|_{\Gamma_0} \times \boldsymbol{n} = \boldsymbol{f}$ and $\mathbf{curl}\, \boldsymbol{E}|_{\Gamma_0} \times \boldsymbol{n} = \boldsymbol{g}$.*

The uniqueness question for our inverse problem reads as follows. Given a frequency $\omega > 0$ and two pairs of admissible coefficients $(\varepsilon_j, \sigma_j)$, $j \in \{1, 2\}$, does $C(\varepsilon_1, \sigma_1; \Gamma_0) = C(\varepsilon_2, \sigma_2; \Gamma_0)$ imply $\varepsilon_1 = \varepsilon_2$ and $\sigma_1 = \sigma_2$ in Ω? A uniqueness result for partial data is stated in [4], where geometrical conditions are imposed on the nonaccessible part Γ_1, which is supposed to be part of either a plane or a sphere. In [3], these geometrical conditions are relaxed. The boundary of the domain

is assumed $\mathcal{C}^{1,1}$ and a perfect conducting boundary condition is considered: $\boldsymbol{E}|_{\Gamma_1} \times \boldsymbol{n} = 0$. This hypothesis can be restrictive in applications. The result stated in Theorem 2.3 can be seen as an improvement of these results, as neither geometrical nor boundary conditions are imposed on the nonaccessible part. The idea behind Theorem 2.3 is simple and new, and uses results from [3] and [5].

Theorem 2.3. *Let $\omega > 0$. Assume that $(\varepsilon_j, \sigma_j)$, $j \in \{1, 2\}$, are two pairs of admissible coefficients (see Definition 2.1) such that $\varepsilon_1 = \varepsilon_2$ and $\sigma_1 = \sigma_2$ in $\bar{\mathcal{V}}$ where $\mathcal{V}$ is a tubular neighborhood of Γ. Then $C(\varepsilon_1, \sigma_1; \Gamma_0) = C(\varepsilon_2, \sigma_2; \Gamma_0)$ implies $\varepsilon_1 = \varepsilon_2$ and $\sigma_1 = \sigma_2$ in Ω.*

Proof. We begin to prove that, under these hypotheses, Cauchy data sets coincide not only on Γ_0, but on the whole boundary Γ. To this end, consider a couple $(\boldsymbol{f}, \boldsymbol{g}) \in C(\varepsilon_1, \sigma_1; \Gamma)$. Then, there exists $\boldsymbol{E}_1 \in H(\mathbf{curl})$ satisfying

$$\left\{ \begin{array}{rcll} \mathbf{curl}\,\mathbf{curl}\,\boldsymbol{E}_1 - k^2\kappa_1\boldsymbol{E}_1 & = & 0, & \text{in } \Omega, \\ \boldsymbol{E}_1 \times \boldsymbol{n} & = & \boldsymbol{f}, & \text{on } \Gamma, \\ \mathbf{curl}\,\boldsymbol{E}_1 \times \boldsymbol{n} & = & \boldsymbol{g}, & \text{on } \Gamma, \end{array} \right.$$

where $\kappa_1 \coloneqq (\varepsilon_1 + i\sigma_1/\omega)/\varepsilon_0$. Since the boundary conditions are obviously satisfied on the accessible part Γ_0, we get $(\boldsymbol{f}, \boldsymbol{g}) \in C(\varepsilon_1, \sigma_1; \Gamma_0)$. Thus, $(\boldsymbol{f}, \boldsymbol{g}) \in C(\varepsilon_2, \sigma_2; \Gamma_0) = C(\varepsilon_1, \sigma_1; \Gamma_0)$ by assumption. Therefore, there is a field $\boldsymbol{E}_2 \in H(\mathbf{curl})$ such that

$$\left\{ \begin{array}{rcll} \mathbf{curl}\,\mathbf{curl}\,\boldsymbol{E}_2 - k^2\kappa_2\boldsymbol{E}_2 & = & 0, & \text{in } \Omega, \\ \boldsymbol{E}_2 \times \boldsymbol{n} & = & \boldsymbol{f}, & \text{on } \Gamma_0, \\ \mathbf{curl}\,\boldsymbol{E}_2 \times \boldsymbol{n} & = & \boldsymbol{g}, & \text{on } \Gamma_0, \end{array} \right.$$

where $\kappa_2 \coloneqq (\varepsilon_2 + i\sigma_2/\omega)/\varepsilon_0$. Note that the boundary conditions are only satisfied on Γ_0. Now, we define $\boldsymbol{E} \coloneqq \boldsymbol{E}_1 - \boldsymbol{E}_2$. In the neighborhood $\mathcal{V}$ of Γ, $\boldsymbol{E}$ then satisfies

$$\left\{ \begin{array}{rcll} \mathbf{curl}\,\mathbf{curl}\,\boldsymbol{E} - k^2\kappa\boldsymbol{E} & = & 0, & \text{in } \mathcal{V}, \\ \boldsymbol{E} \times \boldsymbol{n} & = & 0, & \text{on } \Gamma_0, \\ \mathbf{curl}\,\boldsymbol{E} \times \boldsymbol{n} & = & 0, & \text{on } \Gamma_0, \end{array} \right.$$

where $\kappa \coloneqq \kappa_1 = \kappa_2$ by assumption on $\mathcal{V}$. We then apply [3, Lemma 5.4, ii] which yields $\boldsymbol{E} \equiv 0$ in $\bar{\mathcal{V}}$. Consequently, we get $\boldsymbol{E}_2 \times \boldsymbol{n} = \boldsymbol{E}_1 \times \boldsymbol{n} = \boldsymbol{f}$ and $\mathbf{curl}\,\boldsymbol{E}_2 \times \boldsymbol{n} = \mathbf{curl}\,\boldsymbol{E}_1 \times \boldsymbol{n} = \boldsymbol{g}$ on the whole boundary Γ. Then, $(\boldsymbol{f}, \boldsymbol{g})$ belongs to the Cauchy data set $C(\varepsilon_2, \sigma_2; \Gamma)$. Changing the roles of $(\varepsilon_1, \sigma_1)$ and $(\varepsilon_2, \sigma_2)$ proves that

$$C(\varepsilon_1, \sigma_1; \Gamma) = C(\varepsilon_2, \sigma_2; \Gamma).$$

Now, we infer from the assumptions on the coefficients that $\partial^\alpha\varepsilon_1 = \partial^\alpha\varepsilon_2$ and $\partial^\alpha\sigma_1 = \partial^\alpha\sigma_2$ on the boundary Γ for any multi-index $\alpha \in \mathbb{N}^3$ such that $|\alpha| \leq 1$. These properties are the assumptions of the global uniqueness theorem of Caro and Zhou (see [5, Theorem 1.1]). This gives $\varepsilon_1 = \varepsilon_2$ and $\sigma_1 = \sigma_2$ in Ω and completes the proof. ■

3 Data transmission

In this section, we are interested in the data completion problem for Maxwell equation. The entry data for our inverse problem is the knowledge of the tangential trace $\boldsymbol{g}_D \coloneqq \boldsymbol{E} \times \boldsymbol{n}$ on the accessible part Γ_0, with $\boldsymbol{E}$ being the electric field resulting from the boundary source term $\boldsymbol{g}_N \coloneqq \mathbf{curl}\,\boldsymbol{E} \times \boldsymbol{n}$. The question of data completion then reads as follow: how can we compute the missing data, that is $\boldsymbol{E} \times \boldsymbol{n}$ on the whole boundary Γ?

As the propagation of the electric field inside Ω is modeled by (1), it seems natural to consider the following Cauchy problem:

$$\left\{ \begin{array}{rcll} \mathbf{curl}\,\mathbf{curl}\,\boldsymbol{E} - k^2\kappa\boldsymbol{E} & = & 0, & \text{in } \Omega, \\ \boldsymbol{E} \times \boldsymbol{n} & = & \boldsymbol{g}_D, & \text{on } \Gamma_0, \\ \mathbf{curl}\,\boldsymbol{E} \times \boldsymbol{n} & = & \boldsymbol{g}_N, & \text{on } \Gamma_0. \end{array} \right. \tag{2}$$

We could then define the missing boundary data as the traces of the solution of problem (2). However, solving this problem requires the knowledge of the refractive index κ in the whole domain Ω, which is unknown in the context of our inverse problem. To work around this issue, we use the main hypothesis stated on the refractive index: κ is equal to the (known) background refractive index κ_0 in $\mathcal{V}$, the tubular neighborhood of Γ. This allows us to write that $\boldsymbol{E}$ satisfies the same Cauchy problem as defined above, but in $\mathcal{V}$, where the refractive index is known:

$$\left\{\begin{array}{rcll} \mathbf{curl}\,\mathbf{curl}\,\boldsymbol{E} - k^2\kappa_0\boldsymbol{E} & = & 0, & \text{in } \mathcal{V}, \\ \boldsymbol{E}\times\boldsymbol{n} & = & \boldsymbol{g}_D, & \text{on } \Gamma_0, \\ \mathbf{curl}\,\boldsymbol{E}\times\boldsymbol{n} & = & \boldsymbol{g}_N, & \text{on } \Gamma_0. \end{array}\right. \tag{3}$$

From [3, Lemma 5.4, ii], we know that, if problem (3) admits a solution, then it is unique. However, Cauchy problems are known to be ill-posed [1, 2]. Then, in order to solve problem (3) numerically, it is necessary to regularize it. In [7], we proposed to adapt the quasi-reversibility method to Maxwell's equations to solve problem (3). In particular, we proved the convergence of the relaxed and regularized formulation to the solution of this Cauchy problem in the case of noisy data. This method gives satisfying results. However, the question of how to choose the involved penalization parameter remains open: in the mentioned paper, we used the method of L-curves, and numerical experiments show that it is indeed promising, but there is no theoretical results to prove its convergence. Moreover, from a numerical point of view, using a penalization parameter that can be very small leads to linear systems that can be difficult to solve, especially in 3D domains.

As an alternative, we propose here to use the iterated quasi-reversibility method, introduced in [8]. To this end, we introduce the auxiliary unknown $\boldsymbol{F} \coloneqq \mathbf{curl}\,\boldsymbol{E}$. In order to keep simple notations, we describe here only the 3D case. However, the method can also be written in 2D in a similar way, adapting the spaces by taking into account that there are two **curl** operators in this case. Then, problem (3) can be written:

$$\left\{\begin{array}{rcll} \mathbf{curl}\,\boldsymbol{F} - k^2\kappa_0\boldsymbol{E} & = & 0, & \text{in } \mathcal{V}, \\ \mathbf{curl}\,\boldsymbol{E} - \boldsymbol{F} & = & 0, & \text{in } \mathcal{V}, \\ \boldsymbol{E}\times\boldsymbol{n} & = & \boldsymbol{g}_D, & \text{on } \Gamma_0, \\ \boldsymbol{F}\times\boldsymbol{n} & = & \boldsymbol{g}_N, & \text{on } \Gamma_0. \end{array}\right. \tag{4}$$

To take into account potential noise, both boundary data $\boldsymbol{g}_D$ and $\boldsymbol{g}_N$ are assumed to belong to $L^2(\Gamma_0)^3$. It is then natural to look for $\boldsymbol{E}$ and $\boldsymbol{F}$ in

$$\tilde{H}(\mathbf{curl}) \coloneqq \{\boldsymbol{u} \in L^2(\mathcal{V})^3 \ ; \ \mathbf{curl}\,\boldsymbol{u} \in L^2(\mathcal{V})^3 \text{ and } \boldsymbol{u}\times\boldsymbol{n} \in L^2(\Gamma_0)^3\},$$

which is a Hilbert space, endowed with the scalar product

$$\forall(\boldsymbol{u},\boldsymbol{v}) \in \tilde{H}(\mathbf{curl})^2, \quad (\boldsymbol{u},\boldsymbol{v})_{\tilde{H}(\mathbf{curl})} \coloneqq \int_{\mathcal{V}} (\boldsymbol{u}\cdot\bar{\boldsymbol{v}} + \mathbf{curl}\,\boldsymbol{u}\cdot\mathbf{curl}\,\bar{\boldsymbol{v}}) + \int_{\Gamma_0} (\boldsymbol{u}\times\boldsymbol{n})\cdot(\bar{\boldsymbol{v}}\times\boldsymbol{n})$$

and the induced norm $\|\cdot\|^2_{\tilde{H}(\mathbf{curl})} \coloneqq (\cdot,\cdot)_{\tilde{H}(\mathbf{curl})}$.

Let $\mathcal{X} \coloneqq \tilde{H}(\mathbf{curl})^2$ and $\mathcal{Y} \coloneqq L^2(\mathcal{V})^3 \times L^2(\mathcal{V})^3 \times L^2(\Gamma_0)^3 \times L^2(\Gamma_0)^3$. These are Hilbert spaces endowed with their respective graph norms. Let us introduce the operator

$$\begin{array}{rccl} A\colon & \mathcal{X} & \to & \mathcal{Y} \\ & (\boldsymbol{E},\boldsymbol{F}) & \mapsto & (\mathbf{curl}\,\boldsymbol{F} - k^2\kappa_0\boldsymbol{E}, \mathbf{curl}\,\boldsymbol{E} - \boldsymbol{F}, \boldsymbol{E}|_{\Gamma_0}\times\boldsymbol{n}, \boldsymbol{F}|_{\Gamma_0}\times\boldsymbol{n}) \end{array}$$

so that problem (4) can be rewritten:

$$\text{Find } \boldsymbol{x} = (\boldsymbol{E},\boldsymbol{F}) \in \mathcal{X} \text{ such that } A\boldsymbol{x} = \boldsymbol{y} \coloneqq (0,0,\boldsymbol{g}_D,\boldsymbol{g}_N) \in \mathcal{Y}.$$

Proposition 3.1. *The operator A is linear, continuous, one-to-one, not onto and has a dense range.*

Proof. It is clear that A is linear and continuous. As the Cauchy problem (3) admits at most one solution but may have no solution, A is one-to-one but not onto. Let us prove that its range

is dense in $\mathcal{Y}$. To this end, we will prove that $\mathrm{Im}(A)^\perp = \{0\}$. Let $\boldsymbol{y} = (\boldsymbol{u}, \boldsymbol{v}, \boldsymbol{f}, \boldsymbol{g}) \in \mathrm{Im}(A)^\perp$. In other words, we have :

$$\forall (\boldsymbol{E}, \boldsymbol{F}) \in \mathcal{X}, \quad (A(\boldsymbol{E}, \boldsymbol{F}), (\boldsymbol{u}, \boldsymbol{v}, \boldsymbol{f}, \boldsymbol{g}))_{\mathcal{Y}} = 0,$$

which reads:

$$\forall (\boldsymbol{E}, \boldsymbol{F}) \in \mathcal{X}, \int_{\mathcal{V}} ((\mathbf{curl}\, \boldsymbol{F} - k^2 \kappa_0 \boldsymbol{E}) \cdot \bar{\boldsymbol{u}} + (\mathbf{curl}\, \boldsymbol{E} - \boldsymbol{F}) \cdot \bar{\boldsymbol{v}}) + \int_{\Gamma_0} ((\boldsymbol{E} \times \boldsymbol{n}) \cdot \bar{\boldsymbol{f}} + (\boldsymbol{F} \times \boldsymbol{n}) \cdot \bar{\boldsymbol{g}}) = 0.$$

We first consider $\boldsymbol{F} \in \mathcal{C}_c^\infty(\mathcal{V})^3$ and $\boldsymbol{E} = 0$, which yields

$$\int_{\mathcal{V}} (\mathbf{curl}\, \boldsymbol{F} \cdot \bar{\boldsymbol{u}} - \boldsymbol{F} \cdot \bar{\boldsymbol{v}}) = 0.$$

An integration by parts then gives $\mathbf{curl}\, \boldsymbol{u} = \boldsymbol{v}$ in $\mathcal{V}$. As $\boldsymbol{v} \in L^2(\mathcal{V})^3$, this yields $\boldsymbol{u} \in H(\mathbf{curl}; \mathcal{V})$. By considering $\boldsymbol{E} \in \mathcal{C}_c^\infty(\mathcal{V})^3$ and $\boldsymbol{F} = 0$, a similar argument gives $\mathbf{curl}\, \boldsymbol{v} = k^2 \overline{\kappa_0} \boldsymbol{u}$ and then $\boldsymbol{v} \in H(\mathbf{curl}; \mathcal{V})$. Now, we take $\boldsymbol{E} = 0$ and $\boldsymbol{F} \in \tilde{H}(\mathbf{curl})$. An integration by parts yields

$$\langle \boldsymbol{F} \times \boldsymbol{n}, \boldsymbol{n} \times (\boldsymbol{u} \times \boldsymbol{n}) \rangle_{\partial \mathcal{V}} = \int_{\Gamma_0} (\boldsymbol{F} \times \boldsymbol{n}) \cdot \bar{\boldsymbol{g}}.$$

Then, we obtained:

$$\boldsymbol{g} = \begin{cases} \boldsymbol{n} \times (\boldsymbol{u} \times \boldsymbol{n}), & \text{on } \Gamma_0, \\ 0, & \text{on } \partial \mathcal{V} \setminus \Gamma_0. \end{cases}$$

Similarly, by taking $\boldsymbol{E} \in \tilde{H}(\mathbf{curl})$ and $\boldsymbol{F} = 0$, we get

$$\boldsymbol{f} = \begin{cases} \boldsymbol{n} \times (\boldsymbol{v} \times \boldsymbol{n}), & \text{on } \Gamma_0, \\ 0, & \text{on } \partial \mathcal{V} \setminus \Gamma_0. \end{cases}$$

Grouping all these results together, we obtain that $\boldsymbol{u} \in H(\mathbf{curl}; \mathcal{V})$ satisfies

$$\begin{cases} \mathbf{curl}\, \mathbf{curl}\, \boldsymbol{u} - k^2 \overline{\kappa_0} \boldsymbol{u} &= 0, \quad \text{in } \mathcal{V}, \\ \boldsymbol{u} \times \boldsymbol{n} &= 0, \quad \text{on } \partial \mathcal{V} \setminus \Gamma_0, \\ \mathbf{curl}\, \boldsymbol{u} \times \boldsymbol{n} &= 0, \quad \text{on } \partial \mathcal{V} \setminus \Gamma_0. \end{cases}$$

By uniqueness of the solution to the Cauchy problem, we then have $\boldsymbol{u} \equiv 0$, and then $\boldsymbol{v} \equiv 0$, $\boldsymbol{f} \equiv 0$ and $\boldsymbol{g} \equiv 0$, so $\boldsymbol{y} = 0$, which ends the proof. ■

Let us now introduce the sesquilinear form

$$\begin{array}{rccc} b\colon & \mathcal{X} \times \mathcal{X} & \to & \mathbb{C} \\ & ((\boldsymbol{u}_1, \boldsymbol{v}_1), (\boldsymbol{u}_2, \boldsymbol{v}_2)) & \mapsto & \int_\Omega (\boldsymbol{u}_1 \cdot \bar{\boldsymbol{v}_1} + \boldsymbol{u}_2 \cdot \bar{\boldsymbol{v}_2}). \end{array}$$

It is readily seen that the norm $\sqrt{\|A\cdot\|_{\mathcal{Y}}^2 + b(\cdot,\cdot)}$ is equivalent to $\|\cdot\|_{\mathcal{X}}$. Let $\boldsymbol{y} = (0, 0, \boldsymbol{g}_D, \boldsymbol{g}_N) \in \mathcal{Y}$ be such that problem (4) admits a (unique) solution $(\boldsymbol{E}, \boldsymbol{F})$. For $\delta > 0$, we define the sequence $(\boldsymbol{x}_\delta^M)_{M \in \mathbb{N} \cup \{-1\}}$ by $\boldsymbol{x}_\delta^{-1} \coloneqq 0$ and then, for all $M \in \mathbb{N}$, x_δ^M is the unique element in $\mathcal{X}$ satisfying:

$$\forall \boldsymbol{x} \in \mathcal{X}, \quad (A\boldsymbol{x}_\delta^M, A\boldsymbol{x})_{\mathcal{Y}} + \delta b(\boldsymbol{x}_\delta^M, \boldsymbol{x}) = (\boldsymbol{y}, A\boldsymbol{x})_{\mathcal{Y}} + \delta b(\boldsymbol{x}_\delta^{M-1}, \boldsymbol{x}).$$

Results from [8] then guarantees, using Proposition 3.1, that

$$\lim_{M \to +\infty} \boldsymbol{x}_\delta^M = (\boldsymbol{E}, \boldsymbol{F}).$$

As it has been observed in [7], the error committed when the solution of the Cauchy problem is approximated using the quasi-reversibility method is lower in the interior of the domain $\mathcal{V}$ than on the nonaccessible boundary Γ_1. Then, in view of solving our inverse problem, it seems interesting to not complete the data on the whole boundary Γ, which requires to use the reconstructed field on Γ_1. Instead, we introduce an artificial boundary inside $\mathcal{V}$, $\Gamma_{\mathrm{int}} \coloneqq \partial U$, where U is a open set such that $U \cap \mathcal{V} \neq \emptyset$, as illustrated in Figure 1. The quasi-reversibility method allows us to transmit the partial data from Γ_0 to Γ_{int}: then, we can consider that we have total data on the boundary of the subdomain U.

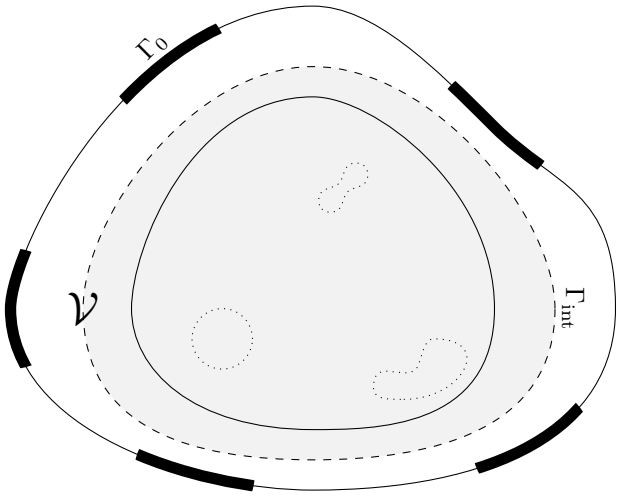

Figure 1: Example of possible configuration for the domain Ω. The accessible part of the boundary Γ_0 is shown as thick parts on $\partial\Omega$. The support of the perturbation is here composed of three parts, delimited by dotted lines. This support does not touch $\mathcal{V}$, the tubular neighborhood where κ is assumed to be known. Finally, Γ_{int} is an artificial boundary, included in $\mathcal{V}$, delimiting an interior domain (here in gray) where data are total.

Remark 3.2. *When using the iterated quasi-reversibility method to approximate the solution of the rewritten Cauchy problem* (4)*, one can observe that the error can be too important to be neglected in high-frequency regimes. One possible workaround, if κ_0 is constant over $\mathcal{V}$, consists in considering $\boldsymbol{F} = \frac{1}{k\sqrt{\kappa_0}}\,\mathbf{curl}\,\boldsymbol{E}$ instead of simply $\boldsymbol{F} = \mathbf{curl}\,\boldsymbol{E}$. This yields the system*

$$\left\{\begin{array}{rcll} \mathbf{curl}\,\boldsymbol{F} - k\sqrt{\kappa_0}\boldsymbol{E} &=& 0, & \text{in } \mathcal{V},\\ \mathbf{curl}\,\boldsymbol{E} - k\sqrt{\kappa_0}\boldsymbol{F} &=& 0, & \text{in } \mathcal{V},\\ \boldsymbol{E}\times\boldsymbol{n} &=& \boldsymbol{g}_D, & \text{on } \Gamma_0,\\ \boldsymbol{F}\times\boldsymbol{n} &=& \frac{1}{k\sqrt{\kappa_0}}\boldsymbol{g}_N, & \text{on } \Gamma_0, \end{array}\right.$$

offering a better precision.

4 Iterated sensitivity equation

From now on, for any admissible refractive index κ, we denote by $\boldsymbol{E}[\kappa]$ the solution of the direct problem

$$\left\{\begin{array}{rcll} \mathbf{curl}\,\mathbf{curl}\,\boldsymbol{E}[\kappa] - k^2\kappa\boldsymbol{E}[\kappa] &=& 0, & \text{in } \Omega,\\ \mathbf{curl}\,\boldsymbol{E}[\kappa]\times\boldsymbol{n} &=& \boldsymbol{g}_N, & \text{on } \Gamma, \end{array}\right. \tag{5}$$

where $\boldsymbol{g}_N$ is the Neumann trace of a given incident wave. Using arguments that can be found in [15], we can prove Proposition 4.1 which will be used in this section. In this statement, we adopt the following notation: for any couple $(a,b) \in (\mathbb{R}^+)^2$,

$$a \lesssim b \iff (\exists C > 0 / a \leq Cb).$$

Proposition 4.1. *Let $\boldsymbol{F} \in L^2(\Omega)^p$ and $\boldsymbol{g} \in Y(\Gamma)'$. The variational formulation of the problem*

$$\left\{\begin{array}{rcll} \mathbf{curl}\,\mathbf{curl}\,\boldsymbol{E} - k^2\kappa\boldsymbol{E} &=& \boldsymbol{F}, & \text{in } \Omega,\\ \mathbf{curl}\,\boldsymbol{E}\times\boldsymbol{n} &=& \boldsymbol{g}, & \text{on } \Gamma, \end{array}\right.$$

reads

$$\left\{\begin{array}{l} \text{Find } \boldsymbol{E} \in H(\mathbf{curl}) \text{ such that}\\ (\mathbf{curl}\,\boldsymbol{E}, \mathbf{curl}\,\boldsymbol{\phi}) - k^2(\kappa\boldsymbol{E}, \boldsymbol{\phi}) = (\boldsymbol{F}, \boldsymbol{\phi}) + \langle \boldsymbol{g}, \boldsymbol{\phi}_T\rangle_\Gamma, \quad \forall \boldsymbol{\phi} \in H(\mathbf{curl}), \end{array}\right.$$

where $(\cdot,\cdot)$ denotes the dot product in $L^2(\Omega)^p$, $\langle\cdot,\cdot\rangle_\Gamma$ denotes the duality bracket from $Y(\Gamma)'$ to $Y(\Gamma)$ and $\boldsymbol{\phi}_T$ is the continuous extension of the map $\boldsymbol{\phi}\mapsto \boldsymbol{n}\times(\boldsymbol{\phi}\times\boldsymbol{n})$. This variational problem admits a unique solution $\boldsymbol{E}\in H(\mathbf{curl})$, depending continuously on $\boldsymbol{F}$ and $\boldsymbol{g}$:

$$\|\boldsymbol{E}\|_{H(\mathbf{curl})} \lesssim \|\boldsymbol{F}\|_0 + \|\boldsymbol{g}\|_{Y(\Gamma)'},$$

where $\|\cdot\|_0$ denotes the $L^2(\Omega)^p$-norm.

We recall here that we are looking for an unknown refractive index which is assumed to be a perturbation of a known background index κ_0. In this section, the support D of this perturbation is fixed and only its amplitude, $a\in\mathbb{R}$, is allowed to vary. We will then denote κ_a the refractive index we are looking for:

$$\kappa_a \coloneqq \kappa_0(1+a\chi_D),$$

where χ_D is the characteristic function of D, for any $a\in\mathbb{R}$ such that κ_a is still an admissible refractive index. The goal of this section is to provide a tool to study small variations around this amplitude. For any given real number h, we then introduce the perturbed refractive index

$$\kappa_{a+h} \coloneqq \kappa_0(1+(a+h)\chi_D) = \kappa_a + h\kappa_0\chi_D.$$

To study these small variations, we introduce the application mapping a refractive index κ_a to the corresponding electric field $\boldsymbol{E}[\kappa_a]$, solution of (5):

$$\begin{array}{rccc} K\colon & \mathbb{R} & \to & H(\mathbf{curl}) \\ & a & \mapsto & \boldsymbol{E}[\kappa_a]. \end{array}$$

Theorem 4.2. *Let $I\subset\mathbb{R}$ be an open interval such that κ_a is admissible for all $a\in I$. Then $K\in\mathcal{C}^\infty(I;H(\mathbf{curl}))$. Moreover, if we denote, for any $a\in I$ and $n\in\mathbb{N}$, $\boldsymbol{E}_a^{(n)}\coloneqq K^{(n)}(a)$ the n-th derivative of K at point a, then $\boldsymbol{E}_a^{(0)}=\boldsymbol{E}[\kappa_a]$ and, for all $n\in\mathbb{N}^*$, $\boldsymbol{E}_a^{(n)}$ is the unique solution of the iterated sensitivity equation:*

$$\left\{\begin{array}{l} \text{Find } \boldsymbol{E}_a^{(n)}\in H(\mathbf{curl}) \text{ such that} \\ (\mathbf{curl}\,\boldsymbol{E}_a^{(n)},\mathbf{curl}\,\boldsymbol{\phi}) - k^2(\kappa_a\boldsymbol{E}_a^{(n)},\boldsymbol{\phi}) = nk^2(\kappa_0\chi_D\boldsymbol{E}_a^{(n-1)},\boldsymbol{\phi}), \quad \forall\boldsymbol{\phi}\in H(\mathbf{curl}). \end{array}\right. \tag{$\mathcal{S}$}$$

Proof. Let $a\in I$. As I is an open interval, there exists $h_0>0$ such that $a+h\in I$ for all $h\in\,]-h_0,h_0[$. In the following, h will always be assumed to belong in this interval. We will prove by induction on $n\in\mathbb{N}^*$ that:

$$\|\boldsymbol{E}_{a+h}^{(n-1)}-\boldsymbol{E}_a^{(n-1)}\|_{H(\mathbf{curl})}\lesssim|h|, \quad \|\boldsymbol{E}_{a+h}^{(n-1)}\|_{H(\mathbf{curl})}\lesssim\|\boldsymbol{g}_N\|_\Gamma, \quad \|\tilde{\boldsymbol{E}}_a^{(n)}-\boldsymbol{E}_a^{(n)}\|_{H(\mathbf{curl})}\lesssim|h|, \ (\mathcal{H}_n)$$

where:

$$\forall n\in\mathbb{N}^*, \quad \tilde{\boldsymbol{E}}_a^{(n)}\coloneqq\frac{\boldsymbol{E}_{a+h}^{(n-1)}-\boldsymbol{E}_a^{(n-1)}}{h}.$$

Let begin with the case $n=1$. As $\boldsymbol{E}_a^{(0)}=\boldsymbol{E}[\kappa_a]$ is the weak solution of problem (5), it satisfies (according to Proposition 4.1):

$$(\mathbf{curl}\,\boldsymbol{E}_a^{(0)},\mathbf{curl}\,\boldsymbol{\phi}) - k^2(\kappa_a\boldsymbol{E}_a^{(0)},\boldsymbol{\phi}) = \langle\boldsymbol{g}_N,\boldsymbol{\phi}_T\rangle_\Gamma, \quad \forall\boldsymbol{\phi}\in H(\mathbf{curl}). \tag{6}$$

We can as well write the variational problem satisfied by $\boldsymbol{E}_{a+h}^{(0)}$:

$$(\mathbf{curl}\,\boldsymbol{E}_{a+h}^{(0)},\mathbf{curl}\,\boldsymbol{\phi}) - k^2(\kappa_{a+h}\boldsymbol{E}_{a+h}^{(0)},\boldsymbol{\phi}) = \langle\boldsymbol{g}_N,\boldsymbol{\phi}_T\rangle_\Gamma, \quad \forall\boldsymbol{\phi}\in H(\mathbf{curl}),$$

from which we can directly infer, as a consequence of Proposition 4.1, that $\|\boldsymbol{E}_{a+h}^{(0)}\|_{H(\mathbf{curl})}\lesssim\|\boldsymbol{g}_N\|_\Gamma$. We rewrite this problem using the identity $\kappa_{a+h}=\kappa_a+h\kappa_0\chi_D$:

$$(\mathbf{curl}\,\boldsymbol{E}_{a+h}^{(0)},\mathbf{curl}\,\boldsymbol{\phi}) - k^2(\kappa_a\boldsymbol{E}_{a+h}^{(0)},\boldsymbol{\phi}) = \langle\boldsymbol{g}_N,\boldsymbol{\phi}_T\rangle_\Gamma + k^2h(\kappa_0\chi_D\boldsymbol{E}_{a+h}^{(0)},\boldsymbol{\phi}), \quad \forall\boldsymbol{\phi}\in H(\mathbf{curl}). \tag{7}$$

Computing the difference between (7) and (6) yields:

$$(\mathbf{curl}(\boldsymbol{E}_{a+h}^{(0)}-\boldsymbol{E}_a^{(0)}),\mathbf{curl}\,\boldsymbol{\phi}) - k^2(\kappa_a(\boldsymbol{E}_{a+h}^{(0)}-\boldsymbol{E}_a^{(0)}),\boldsymbol{\phi}) = k^2h(\kappa_0\chi_D\boldsymbol{E}_{a+h}^{(0)},\boldsymbol{\phi}), \quad \forall\boldsymbol{\phi}\in H(\mathbf{curl}). \tag{8}$$

From (8) and Proposition 4.1, we obtain:

$$\|\boldsymbol{E}_{a+h}^{(0)} - \boldsymbol{E}_a^{(0)}\|_{H(\mathbf{curl})} \lesssim k^2|h|\|\kappa_0\chi_D\boldsymbol{E}_{a+h}^{(0)}\|_0 \lesssim |h|\|\boldsymbol{E}_{a+h}^{(0)}\|_{H(\mathbf{curl})} \lesssim |h|,$$

which, in particular, shows that K is continuous at point a. Now, from the definition of $\tilde{\boldsymbol{E}}_a^{(1)}$, using (8) and computing the difference with $(\mathcal{S})$ at rank $n = 1$, we get:

$$(\mathbf{curl}(\tilde{\boldsymbol{E}}_a^{(1)} - \boldsymbol{E}_a^{(1)}), \mathbf{curl}\,\boldsymbol{\phi}) - k^2(\kappa_a(\tilde{\boldsymbol{E}}_a^{(1)} - \boldsymbol{E}_a^{(1)}), \boldsymbol{\phi}) = k^2(\kappa_0\chi_D(\boldsymbol{E}_{a+h}^{(0)} - \boldsymbol{E}_a^{(0)}), \boldsymbol{\phi}), \quad \forall \boldsymbol{\phi} \in H(\mathbf{curl}),$$

from which, once again using Proposition 4.1, we get:

$$\|\tilde{\boldsymbol{E}}_a^{(1)} - \boldsymbol{E}_a^{(1)}\|_{H(\mathbf{curl})} \lesssim \|\boldsymbol{E}_{a+h}^{(0)} - \boldsymbol{E}_a^{(0)}\|_{H(\mathbf{curl})} \lesssim |h|.$$

This shows that

$$\lim_{h\to 0} \frac{K(a+h) - K(a)}{h} = \boldsymbol{E}_a^{(1)}$$

in $H(\mathbf{curl})$.

Now, let $n \in \mathbb{N}^*$ be such that $(\mathcal{H}_n)$ is true. We will show that $K^{(n)}$ is still continuous and differentiable at point a. To this end, let us write the variational problems satisfied by $\boldsymbol{E}_a^{(n)}$ and $\boldsymbol{E}_{a+h}^{(n)}$:

$$\begin{aligned}(\mathbf{curl}\,\boldsymbol{E}_a^{(n)}, \mathbf{curl}\,\boldsymbol{\phi}) - k^2(\kappa_a\boldsymbol{E}_a^{(n)}, \boldsymbol{\phi}) &= nk^2(\kappa_0\chi_D\boldsymbol{E}_a^{(n-1)}, \boldsymbol{\phi}), \quad \forall \boldsymbol{\phi} \in H(\mathbf{curl}),\\ (\mathbf{curl}\,\boldsymbol{E}_{a+h}^{(n)}, \mathbf{curl}\,\boldsymbol{\phi}) - k^2(\kappa_{a+h}\boldsymbol{E}_{a+h}^{(n)}, \boldsymbol{\phi}) &= nk^2(\kappa_0\chi_D\boldsymbol{E}_{a+h}^{(n-1)}, \boldsymbol{\phi}), \quad \forall \boldsymbol{\phi} \in H(\mathbf{curl}).\end{aligned}$$

In particular, this gives:

$$\|\boldsymbol{E}_{a+h}^{(n)}\|_{H(\mathbf{curl})} \lesssim \|\boldsymbol{E}_{a+h}^{(n-1)}\|_{H(\mathbf{curl})} \lesssim \|\boldsymbol{g}_N\|_\Gamma,$$

using Proposition 4.1 and $(\mathcal{H}_n)$. As in the case $n = 1$, we use the identity $\kappa_{a+h} = \kappa_a + h\kappa_0\chi_D$ to get:

$$\begin{aligned}&(\mathbf{curl}(\boldsymbol{E}_{a+h}^{(n)} - \boldsymbol{E}_a^{(n)}), \mathbf{curl}\,\boldsymbol{\phi}) - k^2(\kappa_a(\boldsymbol{E}_{a+h}^{(n)} - \boldsymbol{E}_a^{(n)}), \boldsymbol{\phi})\\ &\qquad = nk^2(\kappa_0\chi_D(\boldsymbol{E}_{a+h}^{(n-1)} - \boldsymbol{E}_a^{(n-1)}), \boldsymbol{\phi}) + k^2h(\kappa_0\chi_D\boldsymbol{E}_{a+h}^{(n)}, \boldsymbol{\phi}), \quad \forall \boldsymbol{\phi} \in H(\mathbf{curl}).\end{aligned}$$

Then, using $(\mathcal{H}_n)$:

$$\|\boldsymbol{E}_{a+h}^{(n)} - \boldsymbol{E}_a^{(n)}\|_{H(\mathbf{curl})} \lesssim \|\boldsymbol{E}_{a+h}^{(n-1)} - \boldsymbol{E}_a^{(n-1)}\|_{H(\mathbf{curl})} + |h|\|\boldsymbol{E}_{a+h}^{(n)}\|_{H(\mathbf{curl})} \lesssim |h|,$$

and then $K^{(n)}$ is continuous as point a. Using the definition of $\tilde{\boldsymbol{E}}_a^{(n+1)}$ and $(\mathcal{S})$ written at rank $n+1$, we get:

$$\begin{aligned}&(\mathbf{curl}(\tilde{\boldsymbol{E}}_a^{(n+1)} - \boldsymbol{E}_a^{(n+1)}), \mathbf{curl}\,\boldsymbol{\phi}) - k^2(\kappa_a(\tilde{\boldsymbol{E}}_a^{(n+1)} - \boldsymbol{E}_a^{(n+1)}), \boldsymbol{\phi})\\ &\qquad = nk^2(\kappa_0\chi_D(\tilde{\boldsymbol{E}}_a^{(n)} - \boldsymbol{E}_a^{(n)}), \boldsymbol{\phi}) + k^2(\kappa_0\chi_D(\boldsymbol{E}_{a+h}^{(n)} - \boldsymbol{E}_a^{(n)}), \boldsymbol{\phi}), \quad \forall \boldsymbol{\phi} \in H(\mathbf{curl}).\end{aligned}$$

Then, as usual, we use Proposition 4.1 and $(\mathcal{H}_n)$ to obtain

$$\|\tilde{\boldsymbol{E}}_a^{(n+1)} - \boldsymbol{E}_a^{(n+1)}\|_{H(\mathbf{curl})} \lesssim |h|,$$

which concludes the proof. ■

As we are interested in the tangential trace of the electric field, it is natural to also define the application mapping the amplitude of the perturbation to the trace of the corresponding field:

$$\begin{array}{rccc} K_t\colon & \mathbb{R} & \to & Y(\Gamma) \\ & a & \mapsto & \gamma_t(\boldsymbol{E}[\kappa_a]). \end{array}$$

The following result is a direct consequence of Theorem 4.2 and of the fact that γ_t is linear and continuous from $H(\mathbf{curl})$ to $Y(\Gamma)$.

Corollary 4.3. *Let $I \subset \mathbb{R}$ be an open interval such that κ_a is admissible for all $a \in I$. Then $K_t \in \mathcal{C}^\infty(I; Y(\Gamma))$. Moreover, for any $a \in I$ and $n \in \mathbb{N}$, we have $K_t^{(n)}(a) = \gamma_t \circ K^{(n)}(a)$.*

5 A linearized cost functional

We recall that our goal in this paper is to reconstruct a refractive index κ_{ex}. When Ω is illuminated by a wave of trace $\boldsymbol{g}_N$, the electric field $\boldsymbol{E}[\kappa_{\text{ex}}]$ propagating inside Ω is solution of problem (5). In the context of our inverse problem, $\boldsymbol{E}[\kappa_{\text{ex}}]$ is unknown in Ω. Instead, we have access to its tangential trace $\boldsymbol{E}[\kappa_{\text{ex}}] \times \boldsymbol{n}$ on Γ_0, the accessible part of the boundary. To solve this inverse problem, a natural approach is to find κ minimizing the cost functional

$$\mathcal{J}\colon \kappa \mapsto \frac{1}{2}\|\boldsymbol{E}[\kappa_{\text{ex}}] \times \boldsymbol{n} - \boldsymbol{E}[\kappa] \times \boldsymbol{n}\|^2_{\Gamma_0},$$

measuring the distance between the measurements and the predictions of the direct problem. Unfortunately, trying to minimize $\mathcal{J}$ without any regularization leads to poor results (see for example [11, Section 6.3]). To regularize this functional, we will first recall that we are assuming that κ_{ex} is a perturbation of a known background refractive index κ_0. Noting D_{ex} the support of this perturbation and $a_{\text{ex}} \in \mathbb{R}$ its amplitude, we have:

$$\kappa_{\text{ex}} = \kappa_0(1 + a_{\text{ex}}\chi_{D_{\text{ex}}}).$$

Our goal is then to retrieve a_{ex} and D_{ex}, which is then equivalent to the reconstruction of κ_{ex}.

The applications K and K_t defined in Section 4 can actually be defined for any support of perturbation D. To highlight this dependency, we rename them to K_D and $K_{D,t}$: each choice a support defines a new couple of applications. This notation allows us to define a first regularization of $\mathcal{J}$ where we are explicitly looking for a perturbation of κ_0:

$$\mathcal{J}_r\colon (D, a) \mapsto \frac{1}{2}\|\boldsymbol{E}[\kappa_{\text{ex}}] \times \boldsymbol{n} - K_{D,t}(a)\|^2_{\Gamma_0}.$$

This naturally regularizes the cost functional by reducing the size of the set of allowed refractive indices. However, evaluating $\mathcal{J}_r$ still requires solving problem (5), each time with a different refractive index. This means that, each time we evaluate $\mathcal{J}_r$ numerically, we have a new matrix to inverse, which can lead to high computational cost and time. We propose here a way to work around this issue by assuming that the amplitude of the perturbation is such that $|a| < 1$. Then, we can use Corollary 4.3. For any fixed support D, as $K_{D,t}$ is $\mathcal{C}^\infty$, it admits a Taylor expansion at any order $N \in \mathbb{N}$:

$$K_{D,t}(a) = \sum_{n=0}^{N} \frac{a^n}{n!} K^{(n)}_{D,t}(0) + o(a^N).$$

It is then possible to choose $N \in \mathbb{N}^*$ large enough so that $o(a^N)$ can be neglected and:

$$K_{D,t}(a) \approx K_{D,t}(0) + \sum_{n=1}^{N} \frac{a^n}{n!} K^{(n)}_{D,t}(0).$$

The idea is then simply to replace the term $K_{D,t}(a)$ in the expression of $\mathcal{J}_r$ by this truncated expansion:

$$J\colon (D, a) \mapsto \frac{1}{2}\left\|\boldsymbol{E}[\kappa_{\text{ex}}] \times \boldsymbol{n} - \boldsymbol{E}[\kappa_0] \times \boldsymbol{n} - \sum_{n=1}^{N} \frac{a^n}{n!} K^{(n)}_{D,t}(0)\right\|^2_{\Gamma_0}.$$

As the background refractive index κ_0 is assumed to be known, $\boldsymbol{E}[\kappa_0]$ can always be computed and we can equivalently say that our entry data in our inverse problem is $\delta\boldsymbol{E} \times \boldsymbol{n} \coloneqq \boldsymbol{E}[\kappa_{\text{ex}}] \times \boldsymbol{n} - \boldsymbol{E}[\kappa_0] \times \boldsymbol{n}$. One can notice that the system required to be solved to compute the derivatives $K^{(n)}_{D,t}(0)$, for $n \in \mathbb{N}^*$ is the same as the one for $\boldsymbol{E}[\kappa_0]$, that is problem (5) with the background refractive index κ_0, for any support D or amplitude a. It is then faster to evaluate numerically J than $\mathcal{J}_r$, as long as a factorization (e.g. an LU decomposition) of the matrix is stored.

6 Numerical results

6.1 A complete inversion procedure

In this section, we test the reconstruction of a refractive index κ_{ex} in different configurations. We assume that κ_{ex} is a perturbation of a known background refractive index κ_0. In all tests, the support of the perturbation D_{ex} is assumed to be a ball contained in $\Omega \setminus \bar{\mathcal{V}}$ where $\mathcal{V}$ will be a given tubular neighborhood of Γ. The amplitude of the perturbation is a real constant a_{ex}. With these notations, we are then looking for D_{ex} and a_{ex} such that:

$$\kappa_{\text{ex}} = \kappa_0(1 + a_{\text{ex}}\chi_{D_{\text{ex}}}).$$

As the support of the perturbation is assumed to be a ball, it is determined by two parameters: its center, denoted $\boldsymbol{x}_{\text{ex}}$ and its radius, denoted r_{ex}.

The data is generated by solving problem (5) with refractive index κ_{ex}, and with $\boldsymbol{g}$ being the Neumann trace of a plane wave $\boldsymbol{E}_{\boldsymbol{\eta}}$ of direction $\boldsymbol{\eta} \in \mathbb{R}^p$ (unitary):

$$\boldsymbol{E}_{\boldsymbol{\eta}} \colon \boldsymbol{x} \mapsto \boldsymbol{\eta}^{\perp} e^{ik\sqrt{\kappa_0}\boldsymbol{\eta}\cdot\boldsymbol{x}},$$

where $\boldsymbol{\eta}^{\perp} \in \mathbb{R}^p$ is a unitary vector orthogonal to $\boldsymbol{\eta}$. Once the electric field $\boldsymbol{E}[\kappa_{\text{ex}}]$ is generated, its tangential trace $\boldsymbol{E}[\kappa_{\text{ex}}] \times \boldsymbol{n}$ is computed on a given part Γ_0 of the boundary. The entry data for the inverse procedure is the collection of the tangential traces obtained from plane waves of different directions $\boldsymbol{\eta}$.

As a first step, we transmit these partial data to a boundary Γ_{int} defined inside $\mathcal{V}$, using the iterated quasi-reversibility method described in Section 3. More precisely, we transmit the difference field to get an approximation of $(\boldsymbol{E}[\kappa_{\text{ex}}] - \boldsymbol{E}[\kappa_0])|_{\Gamma_{\text{int}}} \times \boldsymbol{n}$, used in the rest of the algorithm to reconstruct the perturbation.

In order to reduce the number of unknowns, we use a result from [6]: for $\boldsymbol{z} \in \Gamma_{\text{int}}$, the quantity $|((\boldsymbol{E}[\kappa_{\text{ex}}] - \boldsymbol{E}[\kappa_0]) \times \boldsymbol{n})(\boldsymbol{z})|$ decreases as the distance between $\boldsymbol{z}$ and $\boldsymbol{x}_{\text{ex}}$ increases. In other words, this modulus is controled by a surface peak that can be localized to obtain an approximation of $\hat{\boldsymbol{x}}_{\text{ex}}$, the projection of $\boldsymbol{x}_{\text{ex}}$ on Γ_{int}. Denoting $\hat{\boldsymbol{n}}$ the normal at this point, we then have:

$$\boldsymbol{x}_{\text{ex}} = \hat{\boldsymbol{x}}_{\text{ex}} - d_{\text{ex}}\hat{\boldsymbol{n}},$$

where $d_{\text{ex}} > 0$ is the depth of the perturbation.

Having an approximation of $\hat{\boldsymbol{x}}_{\text{ex}}$ allows to reduce the number of parameters to retrieve to three scalars: the depth of the perturbation, its radius, and its amplitude. For $d > 0$, we note $\boldsymbol{x}(d) = \hat{\boldsymbol{x}} - d\hat{\boldsymbol{n}}$. Let's denote $D(d, r)$ the ball centered at $\boldsymbol{x}(d)$ and of radius r. As a final step of the algorithm, we will then minimize the functional

$$j \colon (d, r, a) \mapsto J(D(d, r), a).$$

In all tests, we minimize in two steps. Let us introduce the functional

$$\tilde{j} \colon (d, r) \mapsto \min_a j(d, r, a).$$

In other words, for a given (fixed) support of perturbation, we are looking for the optimal amplitude, that is the amplitude allowing us to best approach the boundary data. As the parameters d and r are fixed, the functional $j(d, r, \cdot)$ is a simple function from $\mathbb{R}$ to $\mathbb{R}$ and can then be minimized using classical methods. Here, we chose to use a golden section method [13]. To minimize the functional $\tilde{j}$ which is defined from $\mathbb{R}^2$ to $\mathbb{R}$, we chose to apply the Nelder-Mead method [17].

All PDEs are solved with FreeFem++ [10], using edge finite elements of order 1 (see [16]). The meshes are generated with Gmsh [9]. All examples can be reproduced using the code available in the dedicated Git repository [12].

6.2 Unit disk

We begin with a simple case, in two dimensions ($p = 2$). Here, Ω is the unit disk. The tubular neighborhood $\mathcal{V}$ where it is assumed that there is no perturbations is the annulus of outer radius

1 and of inner radius 0.7. The accessible part of the boundary, Γ_0, is the union of 32 patches equally distributed on Γ. We add an artificial boundary Γ_{int} inside $\mathcal{V}$ where the partial data will be transmitted: it is chosen as the circle centered at the origin and of radius 0.8. Then, U is the disk centered at the origin and of radius 0.8. The perturbation that we will want to retrieve is located in the disk centered at point $(-0.4, 0)$ and of radius 0.2. This configuration is illustrated in Figure 2.

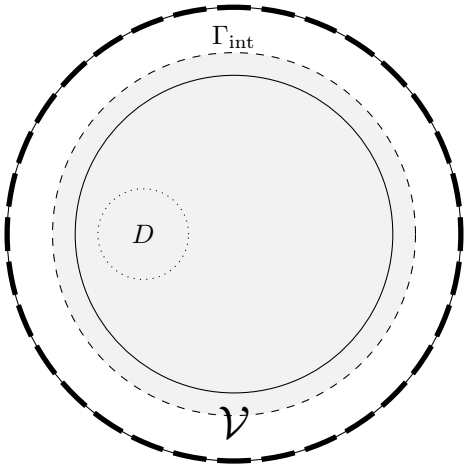

Figure 2: Configuration of the domain Ω for the first numerical test. The thicker parts on the boundary is Γ_0. The artificial boundary is the dashed line, while the dotted line represents the boundary of the support of the perturbation.

We fix the physical constants ω, μ_0 and ε_0 to 1. The background permittivity and conductivity are also set to 1. Then, the background refractive index is here $\kappa_0 \coloneqq 1 + i$. The refractive index that we will want to retrieve is a perturbation of this background index:

$$\kappa_{\text{ex}} \coloneqq \kappa_0(1 + a_{\text{ex}}\chi_{D_{\text{ex}}}),$$

where the support D_{ex} is the disk centered at $\boldsymbol{x}_{\text{ex}} \coloneqq (-0.4, 0)$ and of radius $r_{\text{ex}} \coloneqq 0.2$, and $a_{\text{ex}} \coloneqq 0.1$ is the amplitude. We find that the exact projection of the perturbation on Γ_{int} is $\hat{\boldsymbol{x}}_{\text{ex}} = (-0.8, 0)$. Then, the exact depth is $d_{\text{ex}} = 0.4$.

The synthetic data are generated on a mesh of the unit disk Ω of size $1.37998 \cdot 10^{-2}$, using 74 525 triangles (37 584 vertices and 112 108 edges). We use eight incident waves, of directions $\boldsymbol{\eta}_m \coloneqq (\cos\theta_m, \sin\theta_m)$ with $\theta_m \coloneqq 2\pi\frac{m}{8}$ for $0 \leq m \leq 7$. The data transmission problem is solved on a mesh of the known neighborhood $\mathcal{V}$ of size $2.00013 \cdot 10^{-2}$, using 18 190 triangles (9466 vertices and 27 656 edges). The cost function j is minimized on a mesh of the unit disk of size $4.08549 \cdot 10^{-2}$, using 8691 triangles (4459 vertices and 13 149 edges). In Table 1, we summarize the results obtained in this configuration. The reconstructed refractive index is shown in Figure 3.

Parameter	Exact value	Approximation	Relative error
Center	$(-0.4,\ 0)$	$(-0.37212,\ 0.00482)$	$7.07432 \cdot 10^{-2}$
Radius	0.2	0.21332	$6.65934 \cdot 10^{-2}$
Amplitude	0.1	0.08993	$1.00668 \cdot 10^{-1}$

Table 1: Reconstruction of a spherical perturbation in the unit disk in 2D, with unitary physical parameters.

6.3 3D case

We now propose a 3D equivalent of the previous case. The domain Ω is the unit ball. The known neighborhood $\mathcal{V}$ is the annulus of outer radius 1 and inner radius 0.8. The accessible part Γ_0 is the

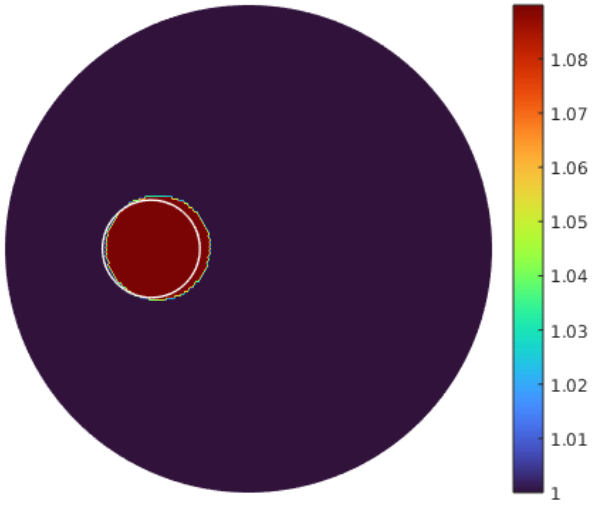

Figure 3: Real part of the reconstructed refractive index in the unit disk. The boundary of the exact support of the perturbation is shown as a white line.

union of 102 patches distributed on the whole boundary Γ. This is illustrated in Figure 4. Inside $\mathcal{V}$, we define the artificial boundary Γ_{int} as the sphere centered at the origin and of radius 0.9. The perturbation is located in the ball centered at point $(-0.4, 0, 0)$ and of radius 0.2.

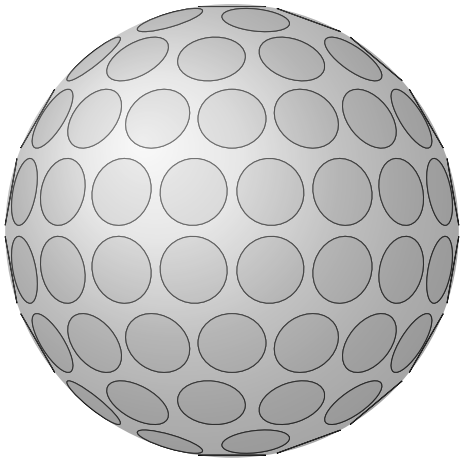

Figure 4: Configuration of the domain Ω in 3D. The accessible part Γ_0 is represented by the patches on the sphere.

As in the 2D case, the physical constants are all fixed to 1, leading to a background refractive index equal to $\kappa_0 = 1 + i$. The amplitude of the perturbation is given by $a_{\text{ex}} \coloneqq 0.2$.

Data are generated on a mesh of the unit ball Ω of size $1.17157 \cdot 10^{-1}$, using 177 809 tetrahedrons (32 488 vertices and 217 291 edges). We use six incident waves of directions

$$\boldsymbol{\eta} \in \{(\pm 1, 0, 0), (0, \pm 1, 0), (0, 0, \pm 1)\}.$$

The data transmission problem is solved on a mesh of $\mathcal{V}$ of size $9.04978 \cdot 10^{-2}$, using 160 156 tetrahedrons (34 520 vertices and 211 511 edges). The cost function j is minimized on a mesh of the unit ball of size $1.57357 \cdot 10^{-1}$, using 63 118 tetrahedrons (12 363 vertices and 79 530 edges). Results are summarized in Table 2 and illustrated in Figure 5.

Parameter	Exact value	Approximation	Relative error
Center	$(-0.4, 0, 0)$	$(-0.35133, -0.03888, -0.02493)$	$1.67741 \cdot 10^{-1}$
Radius	0.2	0.18581	$7.09392 \cdot 10^{-2}$
Amplitude	0.2	0.25589	$2.79469 \cdot 10^{-1}$

Table 2: Reconstruction of a spherical perturbation in the unit ball in 3D, with unitary physical parameters.

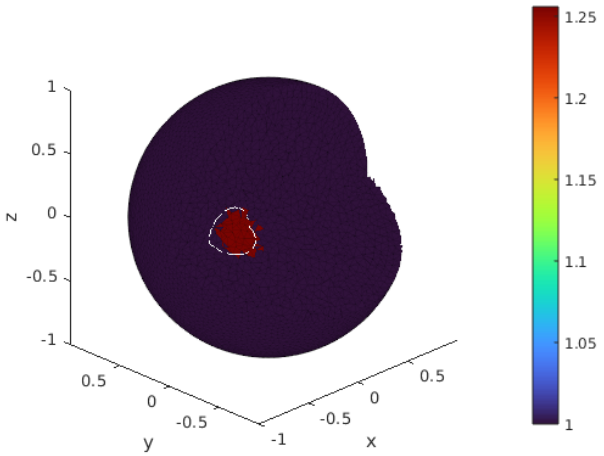

Figure 5: Real part of the reconstructed refractive index in 3D unit ball. The boundary of the exact support of the perturbation is shown as a white line.

6.4 Microwave regime

Coming back to a two-dimensional setting, we now propose a slightly more complicated geometry. Here, the domain Ω represents a head profile. The known neighborhood $\mathcal{V}$ is the region between the boundary of Ω and an ellipse, and we choose a bigger ellipse to represent the artificial boundary Γ_{int}. The accessible part of the boundary is the union of 34 patches. The perturbation will be located in the disk centered at $(0.2, 0.5)$ and of radius 0.1. This configuration is illustrated in Figure 6.

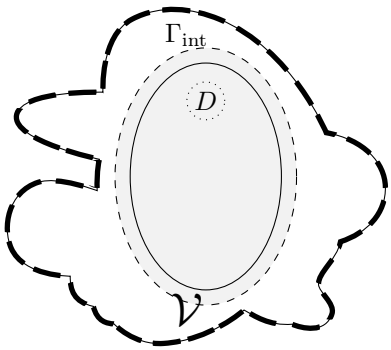

Figure 6: Configuration of the domain Ω for the head profile. The thicker parts on the boundary is Γ_0. The artificial boundary is the dashed line, while the dotted line represents the boundary of the support of the perturbation.

We use here the common definitions of the physical constants. The permittivity in vacuum is then set to $\varepsilon_0 \coloneqq 8.854 \cdot 10^{-12}\,\mathrm{F} \cdot \mathrm{m}^{-1}$ and the magnetic permeability of the vacuum is set to $\mu_0 \coloneqq 4\pi \cdot 10^{-7}\,\mathrm{H} \cdot \mathrm{m}^{-1}$. We choose a frequency in the microwave regime, that is $\omega \coloneqq 10^8\,\mathrm{Hz}$.

The background permittivity of the medium is fixed to $\varepsilon := 10^{-10}\,\mathrm{F}\cdot\mathrm{m}^{-1}$ and its background conductivity is fixed to $\sigma := 0.33\,\mathrm{S}\cdot\mathrm{m}^{-1}$. This yields $\kappa_0 \approx 1.1294\cdot 10^1 + 3.7271\cdot 10^2 i$. As previously, the exact refractive index is a perturbation of this background index:

$$\kappa_{\mathrm{ex}} := \kappa_0(1 + a_{\mathrm{ex}}\chi_{D_{\mathrm{ex}}}),$$

with $a_{\mathrm{ex}} := 0.1$ and D_{ex} the disk centered at $\boldsymbol{x}_{\mathrm{ex}} := (0.2, 0.5)$ and of radius $r_{\mathrm{ex}} := 0.1$.

Data are generated on a mesh of Ω of size $2.80451\cdot 10^{-3}$, using 1 396 929 triangles (700 240 vertices and 2 097 168 edges). We use 16 incident waves, defined in the same way as in the unit disk case (see subsection 6.2). A noise is added to the generated data, using the following procedure. Each degree of freedom of the tangential trace $\boldsymbol{g}_D$ of the field is perturbed by the addition of a random complex number in such a way that

$$\frac{\|\boldsymbol{g}_D^\eta - \boldsymbol{g}_D\|_{0,\Gamma_0}}{\|\boldsymbol{g}_D\|_{0,\Gamma_0}} = \eta,$$

where $\eta > 0$ is the level of noise and $\boldsymbol{g}_D^\eta$ is the noised trace. In this test, we fix this level of noise to $\eta = 0.02$. The data transmission problem is solved on a mesh of $\mathcal{V}$ of size $3.45773\cdot 10^{-3}$, using 622 148 triangles (313 135 vertices and 935 283 edges). The minimization is achieved on a mesh of Ω of size $4.14636\cdot 10^{-2}$, using 7930 triangles (4109 vertices and 12 038 edges). The retrieved parameters are summarized in Table 3, with corresponding refractive index shown in Figure 7.

Parameter	Exact value	Approximation	Relative error
Center	(0.05, 0.4)	(0.05532, 0.38747)	$3.37638\cdot 10^{-2}$
Radius	0.1	0.11305	$1.30478\cdot 10^{-1}$
Amplitude	0.1	0.07549	$2.45094\cdot 10^{-1}$

Table 3: Reconstruction of a spherical perturbation in a head profile in 2D, with realistic physical parameters in the microwave regime.

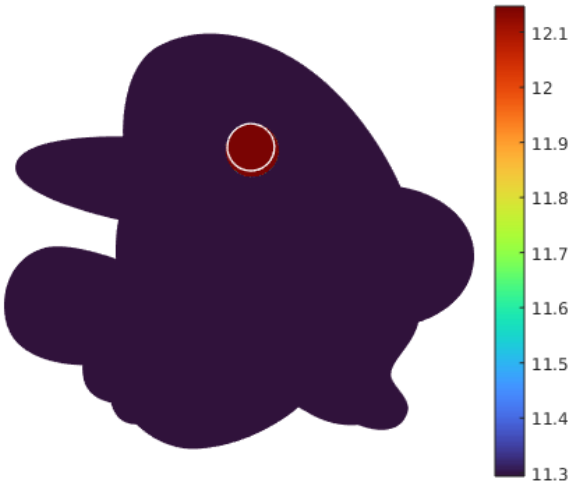

Figure 7: Real part of the reconstructed refractive index in the geometry of a 2D head profile in microwave regime. The boundary of the exact support of the perturbation is shown as a white line.

6.5 Discussion

In all tested configurations, the minimization of the cost function defined in Section 5 leads to good results, with a satisfying precision. One can notice that the locations of the reconstructed

perturbations are always deeper than the exact supports. This can actually be explained by the first step of the procedure, that is the transmission of the boundary data by the quasi-reversibility method. Indeed, in Table 4, we see the parameters retrieved when we use the exact data as entry of the minimization step, instead of the transmitted data, in the case of the unit disk in $\mathbb{R}^2$ (see subsection 6.2). The reconstructed perturbation is shown in Figure 8.

To understand the reason behind this behavior, we compare in Figure 9 the trace of the difference field $(\boldsymbol{E}[\kappa_{\text{ex}}]-\boldsymbol{E}[\kappa_0])\times\boldsymbol{n}$ on Γ_{int} with the trace resulting from the resolution of the transmission problem. It can be observed that the reconstructed surface peak is well-located. However, it has a lower amplitude and occupies more space over the surface. As it has been observed in [6], the space occupied by the surface peak depends on the depth of the perturbation: the deeper a perturbation is, the larger will be the surface peak. As the reconstructed surface peak is larger than the exact one, it is then natural to reconstruct deeper perturbations at the end. It is not clear currently whether or not it is possible to predict the deformation of the peak due to the transmission step in order to correct it and obtain more precise results.

Parameter	Exact value	Approximation	Relative error
Center	$(-0.4,\ 0)$	$(-0.39741,\ 0.00226)$	$8.60097 \cdot 10^{-3}$
Radius	0.2	0.20344	$1.71859 \cdot 10^{-2}$
Amplitude	0.1	0.09784	$2.16249 \cdot 10^{-2}$

Table 4: Reconstruction of a spherical perturbation in the unit disk in 2D, with unitary physical parameters. The transmission step is skipped and exact data are used.

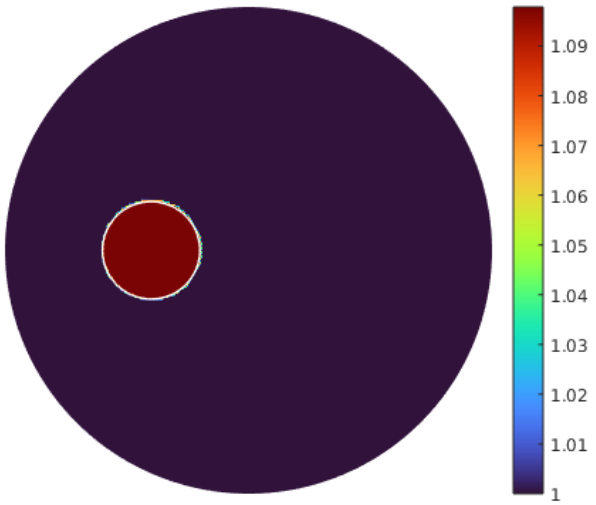

Figure 8: Real part of the reconstructed refractive index in the unit disk with exact data on the whole boundary. The boundary of the exact support of the perturbation is shown as a white line.

6.6 More complex perturbations

One can wonder what the algorithm finds out in cases where some assumptions on the perturbation are not satisfied, that is when its support is not a perfect ball, or when its amplitude is not constant. In Figure 10, we show the results of the complete inversion procedure in such cases. In both tests, the settings are the same as in the unit disk case shown in subsection 6.2, except for two parameters. In the first test, the amplitude of the perturbation is still constant and equal to 0.1, but the support has a shape of a star instead of a ball. In the second test, we go back to a disk, but the amplitude

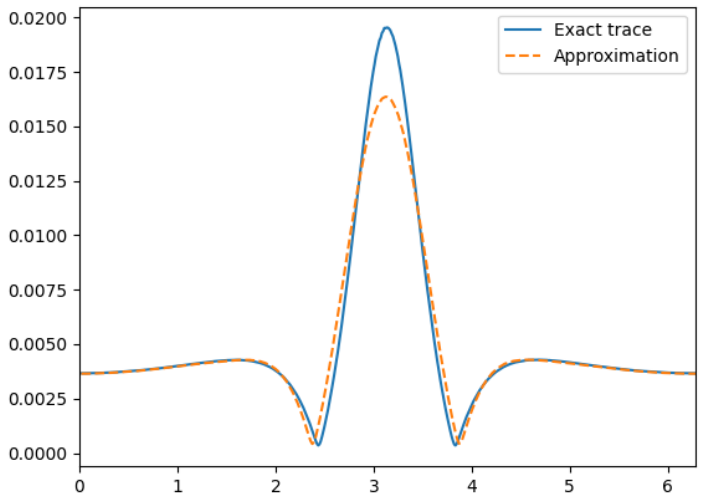

Figure 9: Comparison of the exact tangentiel trace of the difference field $(\boldsymbol{E}[\kappa_{\text{ex}}] - \boldsymbol{E}[\kappa_0]) \times \boldsymbol{n}$ on Γ_{int} and its approximation by the quasi-reversibility method. The circle Γ_{int} is unfolded: the x-axis shows the angle of a point while y-axis shows the value of the modulus of the trace at this point.

is not constant: it is set to

$$a_{\max} e^{-\frac{d^2}{1-d^2}},$$

where $a_{\max} := 0.1$ is the maximum amplitude and d is the distance of the current point to the center of the disk, divided by the radius of the disk. Then, $\kappa \in \mathcal{C}^\infty(\Omega)$, equal to κ_0 outside of the perturbation and to $\kappa_0(1 + a_{\max})$ on the center of the perturbation.

In both cases, the reconstructed perturbation is deeper than the exact support, following the same behavior discussed in the previous section. In the case of the star-shaped perturbation, the algorithm finds an amplitude equal to 0.08996 instead of 0.1. As the procedure is looking for a constant amplitude, it does not retrieve the variations of the second case: it finds a amplitude equal to 0.06180. It is interesting that, in both cases, the procedure provides a rough idea of the perturbation, which could serve as a good initial guess for a more general algorithm, using for instance shape derivatives to capture more complex shapes of supports. This is however beyond the scope of this paper.

7 Concluding remarks

Using the iterated sensitivity equation, we were able to regularize the classical cost functional used to solve the inverse problem we are interested in. The complete inversion procedure provides good results when it comes to the reconstruction of a perturbation from the knowledge of partial surface measurements, even in cases where the shape or amplitude of the perturbation is not what the algorithm is expecting.

In addition to the regularization it provides, the use of an asymptotic expansion is also interesting from a numerical point of view: using a direct solver, the evaluation of this cost functional is faster than the evaluation of the classical one, as it is always the same linear system that needs to be inverted. The same remark applies to the use of the iterated quasi-reversibility: all iterations, for all incident waves, share the same linear system. The limitations of using direct solvers are however well known. In particular, it prevents the use of fine meshes, especially in 3D.

In this paper, we focused on the reconstruction of a single perturbation. Looking for several perturbations should be achievable in a similar way: as it has been proved in [6], each perturbation

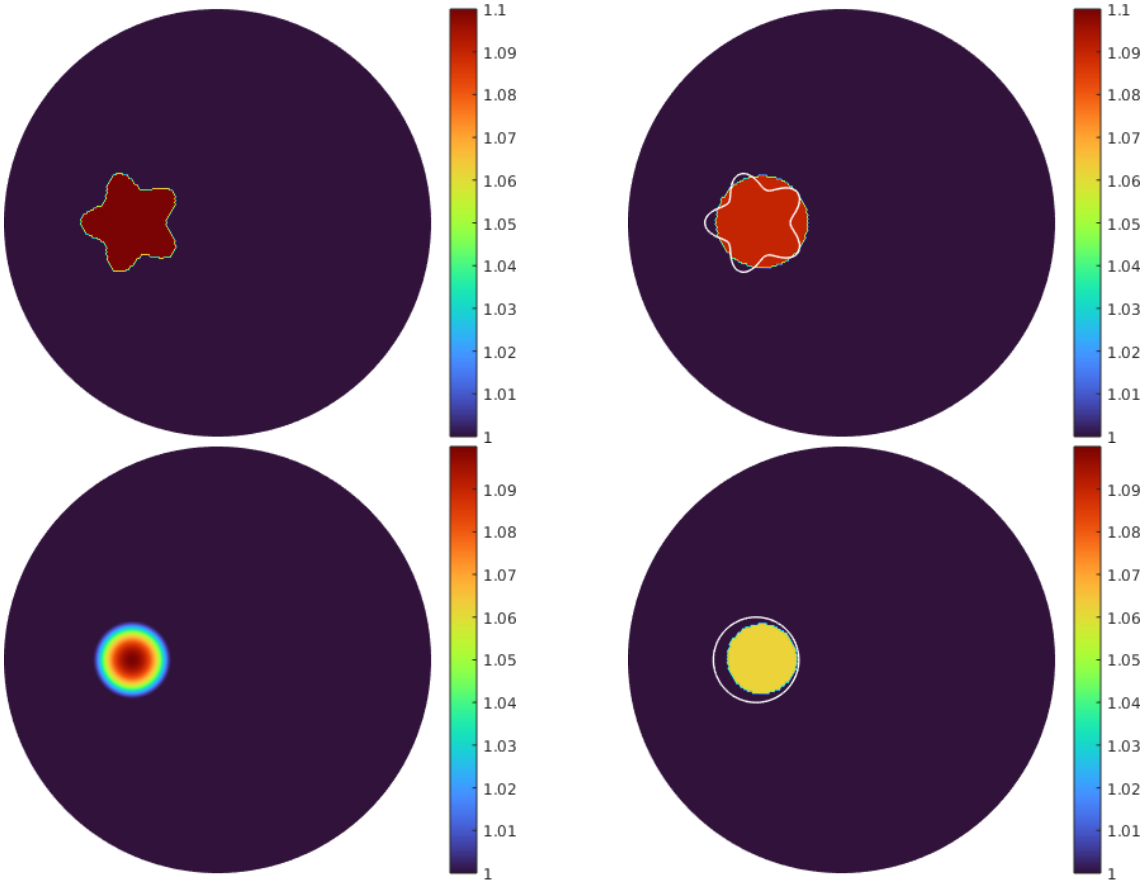

Figure 10: Reconstruction of more complex perturbations in the unit disk in 2D. Top pictures: star-shaped perturbation with constant amplitude. Bottom pictures: disk-shaped perturbation with variable amplitude. Left pictures: real part of the exact refractive index. Right pictures: results of the complete inversion procedures.

will generate its own surface peak. By splitting the trace according to these peaks, it is then possible to apply the reconstruction algorithm separately on each part and recover all perturbations.

Acknowledgements

The author wants to thank M. Darbas, S. Lohrengel and J. Dardé for the kind discussions and valuable comments along this project.

References

[1] Alessandrini G., Rondi L., Rosset E., Vessella S., The stability for the Cauchy problem for elliptic equations. Inverse problems **25** (2009), 123004.

[2] Ben Belgacem F., Why is the Cauchy problem severely ill-posed?. Inverse problems **23** (2007), pp. 823–836.

[3] Brown B.M., Marletta M., Reyes J.M., Uniqueness for an inverse problem in electromagnetism with partial data. Journal of Differential Equations **260**.8 (2016), pp. 6525–6547.

[4] Caro P., On an inverse problem in electromagnetism with local data: stability and uniqueness. Inverse Problems & Imaging **5** (2011), pp. 297–322.

[5] Caro P., Zhou T., Global Uniqueness for an IBVP for the Time-Harmonic Maxwell Equations. Analysis & PDE **7**.2 (2014), pp. 375–405.

[6] Darbas M., Heleine J., Lohrengel S., Sennsitivity analysis for 3D Maxwell's equations and its use in the resolution of an inverse medium problem at fixed frequency. Inverse Problems in Science & Engineering **28**.4 (2020), pp. 459–496, doi:10.1080/17415977.2019.1588896.

[7] Darbas M., Heleine J., Lohrengel S., Numerical resolution by the quasi-reversibility method of a data completion problem for Maxwell's equations. Inverse Problems and Imaging **14**.6 (2020), pp. 1107–1133, doi:10.3934/ipi.2020056.

[8] Dardé J., Iterated quasi-reversibility method applied to elliptic and parabolic data completion problems. Inverse Problems and Imaging **10**.2 (2016), pp. 379–407.

[9] Geuzaine C., Remacle J.-F., Gmsh: a three-dimensional finite element mesh generator with built-in pre- and post-processing facilities. International Journal for Numerical Methods in Engineering **79**.11 (2020), pp. 1309–1331.

[10] Hecht F., New Development in FreeFem++. Journal of Numerical Mathematics **20**.3-4 (2012), pp. 251–265.

[11] Heleine J., Identification de paramètres électromagnétiques par imagerie micro-ondes. Ph.D thesis, Université de Picardie Jules Verne in Amiens, France, 2019.

[12] Heleine J., Reconstruction of perturbations. Git repository, 2023.
https://plmlab.math.cnrs.fr/jheleine/reconstruction-of-perturbations

[13] Kiefer J., Sequential minimax search for a maximum. Proceedings of the American Mathematical Society **4** (1953), pp. 502–506.

[14] Kwon S., Lee S., Recent advances in microwave imaging for breast cancer detection. International Journal of Biomedical Imaging (2016).

[15] Monk P., Finite Element Methods for Maxwell's Equations. Oxford Science Publications, 2003.

[16] Nédélec J.-C., Mixed finite elements in $\mathbb{R}^3$. Numerische Mathematik **50**.1 (1986), pp. 57–81.

[17] Nelder J. A., Mead R., A Simplex Method for Function Minimization. The Computer Journal **7**.4 (1965), pp. 308–313.

[18] Semenov S., Seiser B., Stoegmann E., Auff E., Electromagnetic tomography for brain imaging: From virtual to human brain. 2014 IEEE Conference on Antenna Measurements & Applications (CAMA), IEEE, 2014.

[19] Tournier P.-H., Bonazzoli M., Dolean V., Rapetti F., et al, Numerical modelling and high speed parallel computing: new perspectives for brain strokes detection and monitoring. IEEE Antennas and Propagation Magazine **59**.5 (2017), pp. 98–110.